Ann. Geophys., 24, 1705–1712, 2006
www.ann-geophys.net/24/1705/2006/

Annales Geophysicae

Study of whistler mode instability in Saturn's magnetosphere

R. P. Singhal and A. K. Tripathi

Department of Applied Physics, Institute of Technology, Banaras Hindu University, Varanasi-221 005, India

Received: 31 January 2006 – Revised: 31 March 2006 – Accepted: 13 April 2006 – Published: 3 July 2006

Abstract. A dispersion relation for parallel propagating whistler mode waves has been applied to the magnetosphere of Saturn and comparisons have been made with the observations made by Voyager and Cassini. The effect of hot (suprathermal) electron-density, temperature, temperature anisotropy, and the spectral index parameter, κ, on the temporal growth rate of the whistler mode emission is studied. A good agreement is found with observations. Electron pitch angle and energy diffusion coefficients have been obtained using the calculated temporal growth rates.

Keywords. Magnetospheric physics (Energetic particles, precipitating; Planetary magnetospheres; Plasma waves and instabilities)

1 Introduction

The observations of the plasma wave spectrum observed at Saturn by Voyager 1 were first reported by Gurnett et al. (1981). Whistler mode hiss and chorus emissions were found as Voyager approached the equator at a radial distance of about 5 R_S (R_S is radius of Saturn). Whistler mode emissions within Saturn's magnetosphere were also detected by the plasma wave instruments on Voyager 2 (Scarf et al., 1982). First results from the Cassini Radio and Plasma Wave Science Instrument during the approach and first orbit around Saturn have been reported by Gurnett et al. (2005). Several diffuse emissions were seen at frequencies below f_c (electron cyclotron frequency). These have been identified as whistler mode emissions. The radial distance of these emissions is about 2∼6 R_S. Whistler waves are electromagnetic waves in magnetized plasmas at frequencies below the electron cyclotron frequency. The ionosphere/magnetosphere produces various plasma instabilities which lead to the emission of waves propagating in the whistler mode waves branch. Most of these instabilities are due to anisotropic electron distributions, such as beams, loss-cones, rings and temperature anisotropies. Whistler mode emissions are also triggered by lightning generated whistler. Whistler mode wave-particle interactions are important processes which can lead to wave amplification and precipitation of energetic electrons from the magnetosphere into the lower ionosphere/atmosphere. In this study we investigate the whistler mode driven unstable by the electron temperature anisotropy in the presence of a suprathermal power law tail on the electron population (Mace, 1998). The source of free energy driving the instability is the electron temperature anisotropy, $T_\perp > T_{||}$. We consider only the wave propagation parallel to the magnetic field.

The plasma science experiment during the Voyager encounters with Saturn investigated the low energy plasma electron environment within Saturn's magnetosphere. The electron distribution functions are found to be non-Maxwellian in character; they are composed of a cold (thermal) component with a Maxwellian shape and a hot (suprathermal), non-Maxwellian component (Sittler et al., 1983). Similar characteristics of electron distribution functions have been found during Cassini's initial orbit (Young et al., 2005). The colder component (∼3 to 30 eV) increases in density and decreases in temperature with decreasing radial distance. The hotter component (∼100 to 1000 eV) has the opposite behaviour; it decreases in density and increases in temperature with decreasing radial distance. The hot plasma component can be modelled by a loss-cone, bi-Lorentzian (or kappa) distribution (Summers and Thorne, 1991). In the present work we have investigated the whistler mode instability driven by temperature anisotropy in the hot electron component in the magnetosphere of Saturn and compare our results with the whistler mode wave observations by Voyager and Cassini. We have also calculated the pitch-angle and energy diffusion coefficients from resonant interactions with whistler mode waves using the expressions derived by Lyons (1974), generalized to the temporal growth rates obtained from our calculations.

Correspondence to: R. P. Singhal
(rpsinghal@bhu.ac.in)

Published by Copernicus GmbH on behalf of the European Geosciences Union.

Table 1. Voyager 1 observational data.

Distance	n_c (cm^{-3})	n_h (cm^{-3})	T_c (eV)	T_h (eV)	B_0 (nT)
$R\sim 6\,R_S$	13	1	12	400	80
$R\sim 12\,R_S$	0.34	0.06	25	500	12
$R\sim 18\,R_S$	0.042	0.028	44	600	4.4

Section 2 gives the dispersion relation for parallel propagating whistler mode waves. The plasma parameters in Saturn's magnetosphere and those used in the present study are discussed in Sect. 3. Results of the temporal growth rates are given in Sect. 4. In Sect. 5 we give the calculated normalized pitch angle and energy diffusion coefficients. Finally, in Sect. 6, a brief discussion and the conclusions of the present study are given.

2 Dispersion relation

We consider a plasma consisting of a cold electron component represented by a Maxwellian distribution, a hot electron component given by the bi-Lorentzian loss-cone distribution and a proton component represented by cold and hot components, which are also given by Maxwellian and bi-Lorentzian loss-cone distributions, respectively. The Maxwellian distribution is given by

$$f_\sigma^{\rm M}(v_\perp, v_{||}) = \frac{1}{\pi^{3/2} a_{\perp_\sigma}^2 a_{||_\sigma}} \exp\left(-\frac{v_{||}^2}{a_{||_\sigma}^2} - \frac{v_\perp^2}{a_{\perp_\sigma}^2}\right) \quad (1)$$

with associated perpendicular and parallel thermal speeds

$$a_{\perp\sigma} = (2T_{\perp_\sigma}/m_\sigma)^{1/2}, \qquad a_{||_\sigma} = (2T_{||_\sigma}/m_\sigma)^{1/2} \quad (2)$$

and temperature anisotropy

$$A_\sigma^{\rm M} = \frac{a_{\perp_\sigma}^2}{a_{||_\sigma}^2} - 1. \quad (3)$$

The bi-Lorentzian loss-cone distribution is given by

$$f_\sigma(v_\perp, v_{||}) = \frac{\pi^{-3/2}\Gamma(\kappa+\ell+1)}{\kappa^{3/2}\theta_{\perp_\sigma}^2 \theta_{||_\sigma} \ell! \Gamma(\kappa-1/2)} \left(\frac{v_\perp^2}{\kappa\theta_{\perp\sigma}^2}\right)^\ell \left(1 + \frac{v_\perp^2}{\kappa\theta_{\perp\sigma}^2} + \frac{v_{||}^2}{\kappa\theta_{||\sigma}^2}\right)^{-(\kappa+\ell+1)} \quad (4)$$

The parameter $\theta_{\perp_\sigma}$ and $\theta_{||_\sigma}$ are thermal speeds given by

$$\theta_{\perp_\sigma} = \left(\frac{2\kappa-3}{\kappa}\right)^{1/2} \frac{1}{(\ell+1)^{1/2}} \left(\frac{T_{\perp_\sigma}}{m_\sigma}\right)^{1/2}, \quad (5)$$

$$\theta_{||_\sigma} = \left(\frac{2\kappa-3}{\kappa}\right)^{1/2} \left(\frac{T_{||_\sigma}}{m_\sigma}\right)^{1/2}, \quad (6)$$

and the temperature anisotropy is given by

$$A_\sigma^\kappa = \frac{T_{\perp_\sigma}}{T_{||_\sigma}} - 1 = (\ell+1)\frac{\theta_{\perp_\sigma}^2}{\theta_{||_\sigma}^2} - 1. \quad (7)$$

Employing distributions (1) and (4), the dispersion relation for the parallel propagating R-mode can be written as (Summers and Thorne, 1995; Mace, 1998)

$$\frac{c^2k^2}{\omega^2} = 1 + \sum_\sigma \frac{\omega_{p\sigma}^2}{\omega^2}\left\{A_\sigma + \left[A_\sigma\left(\frac{\omega+\epsilon_\sigma\Omega_\sigma}{k\theta_{||_\sigma}}\right) + \frac{\omega}{k\theta_{||_\sigma}}\right\} \times \frac{(\kappa-1)^{3/2}}{\kappa^{1/2}(\kappa-3/2)} Z_{\kappa-1}\left[\left(\frac{\kappa-1}{\kappa}\right)^{1/2}\frac{\omega+\epsilon_\sigma\Omega_\sigma}{k\theta||_\sigma}\right]. \quad (8)$$

Summation over species σ involved in Eq. (8) is carried out on cold and hot components of electrons and protons. For the cold component $\kappa\to\infty$, $A_\sigma\to A_\sigma^{\rm M}$, $Z_{\kappa-1}\to Z\left(\frac{\omega+\epsilon_\sigma\Omega_\sigma}{k a_{||_\sigma}}\right)$ and $\theta_{||,\perp_\sigma}\to a_{||,\perp_\sigma}$, where ω is the complex wave frequency ($\omega=\omega_r+i\gamma$), $k=|k_{||}|$, $\omega_{p\sigma}$ is the plasma frequency, $\omega_{p\sigma}^2=\frac{4\pi n_{0\sigma} q_\sigma^2}{m_\sigma}$, the cyclotron frequency Ω_σ is given by $\Omega_\sigma=\frac{|q_\sigma|B_0}{m_\sigma c}$, the charge sign is $\epsilon_\sigma=\frac{q_\sigma}{|q_\sigma|}$, κ is the spectral index, ℓ is the loss-cone index. q_σ, m_σ and n_σ are, respectively, particle charge, mass and number density of species σ. c is the speed of light. B_0 is the ambient magnetic field. The function Z_κ, appearing in Eq. (8), is the modified plasma dispersion function of Summers and Thorne (1991) and Z is the plasma dispersion function (Fried and Conte, 1961). Equation (8) is broken into real and imaginary parts and a numerical technique is used to find the real and imaginary components of ω.

3 Plasma parameters within Saturn's magnetosphere

A survey of the low-energy plasma electron environment during the Voyager encounters with Saturn has been given by Sittler et al. (1983). Three fundamentally different plasma regimes have been identified: (1) The hot outer magnetosphere (R=15∼22 R_S), (2) the extended plasma sheet (R=7∼15 R_S), (3) the inner plasma torus (R<7 R_S, where R is the radial distance). Electron densities are ∼10 cm^{-3} in the inner torus and decrease to about ∼3.0 cm^{-3} in the extended plasma sheet and about ∼ 0.04 cm^{-3} in the outer magnetosphere. The hot (suprathermal) component relative

Table 2. Cassini observational data.

Distance	n_c (cm^{-3})	n_h (cm^{-3})	T_c (eV)	T_h (eV)	B_0 (nT)
$R\sim$ 5.5 R_S	14	0.1	20	2000	100
$R\sim$ 3.9 R_S	30	0.1	20	2000	300
$R\sim$ 2.2 R_S	100	0.1	20	2000	1400

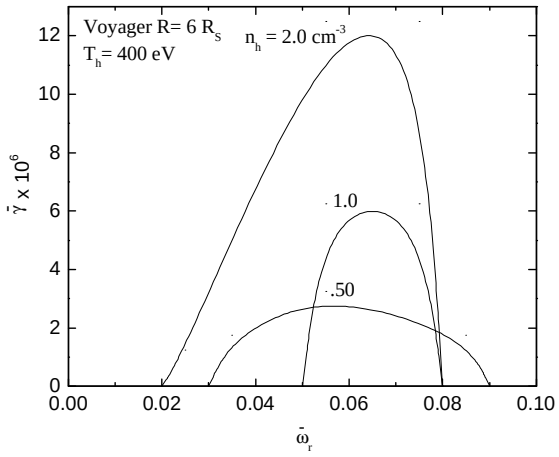

Fig. 1. Normalized temporal growth rate $\bar{\gamma}(=\gamma/\Omega_e)$ versus normalized real frequency $\bar{\omega}_r(=\omega_r/\Omega_e)$ at $R\sim 6\,R_S$. Other plasma parameters are given in Table 1 (Voyager data). Hot (suprathermal) electron density n_h is marked.

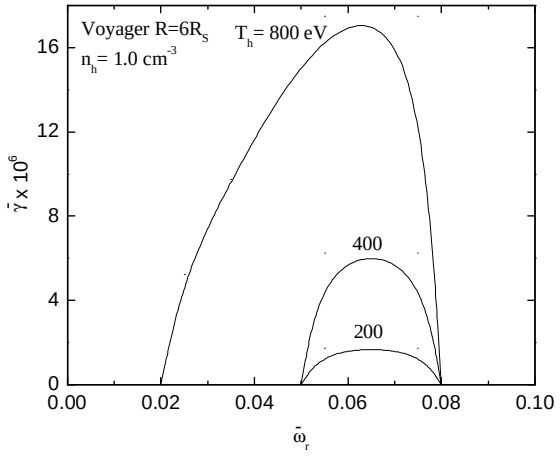

Fig. 2. Same as in Fig. 1 at $R\sim 6\,R_S$. Hot (suprathermal) electron temperature T_h is marked. Other plasma parameters are same as in Fig. 1.

to the cold (thermal) component increases from about 0.1 in the inner torus to about 0.4 in the outer magnetosphere. The cold electron temperature changes from about 10 eV to 40 eV and the hot electron temperature varies from about 400 eV to 600 eV as the radial distance changes from 6 R_S to 18 R_S. The measurements made with the Cassini plasma spectrometer in Saturn's magnetosphere have been reported by Young et al. (2005) and from the Cassini radio and plasma wave instruments by Gurnett et al. (2005). In the inner magnetosphere (R=2 $\sim$7 R_S) electron densities range between 100$\sim$4 cm^{-3}, respectively. The cold electron temperature is about 10$\sim$20 eV and the hot electron temperature is nearly 1000$\sim$2000 eV. The hot (suprathermal) electron density is about 0.1 cm^{-3}. Temporal growth rate calculations for the whistler mode instability have been performed at three radial distances: $R\sim$6 R_S, 12 R_S and 18 R_S using the plasma parameters from the Voyager 1 data given in Table 1.

Subscripts c and h refer to cold (thermal) and hot (suprathermal) electrons. Calculations have been performed by changing the hot electron number density (n_h) and temperature (T_h). Another set of calculations has been performed at three radial distances: $R\sim$5.5 R_S, $R\sim$3.9 R_S and $R\sim$2.2 R_S, using the data set from Cassini given in Table 2.

Cold electrons are assumed isotropic and for hot electrons temperature anisotropy A_h=$T_{\perp h}/T_{||h}-1$=0.1 is used. A value of κ=2 is also used. Calculations have been performed by changing A_h and κ. Protons with a constant hot component temperature 10^4 eV have been included. Other protons parameters are same as for electrons.

4 Temporal growth rates

4.1 Calculation results

In Fig. 1, we show the calculated normalized temporal growth rates ($\bar{\gamma}=\gamma/\Omega_e$) at radial distance 6 R_S. The effect of the changing hot electron number density is shown. At large $n_h\sim$ 2 cm^{-3} the whistler mode emission covers a broad band of frequencies, especially towards lower frequencies, although reducing n_h does not show a systematic trend. In Fig. 2 the effect of hot electron temperature (T_h) is shown. In this case the band width increases towards lower frequencies as T_h is increased from 200 eV to 800 eV. This is in accord with Voyager observations (Sittler et al., 1983). However, it may be noted that for lower values of both parameters, n_h ($\sim$0.5 cm^{-3}) and T_h (200 eV), the calculations produce no whistler mode emissions. In Figs. 3 and 4 we show the

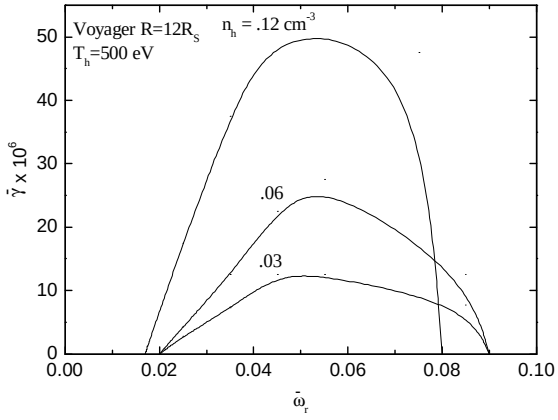

Fig. 3. Same as in Fig. 1 but for $R \sim 12\,R_S$.

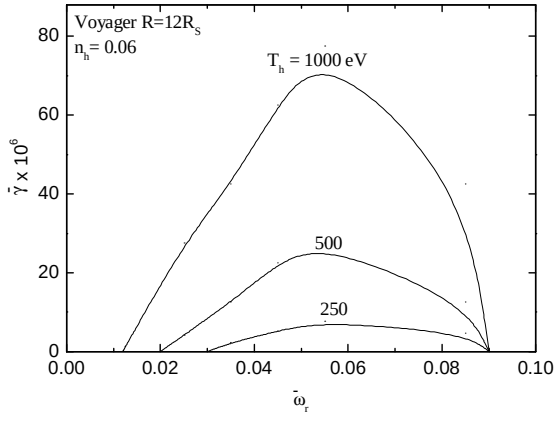

Fig. 4. Same as in Fig. 2 but for $R \sim 12\,R_S$.

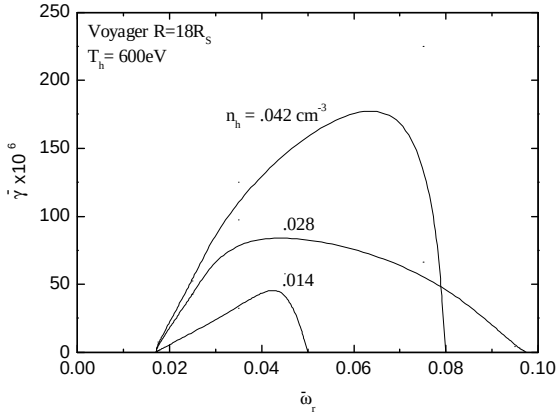

Fig. 5. Same as in Fig. 1 but for $R \sim 18\,R_S$.

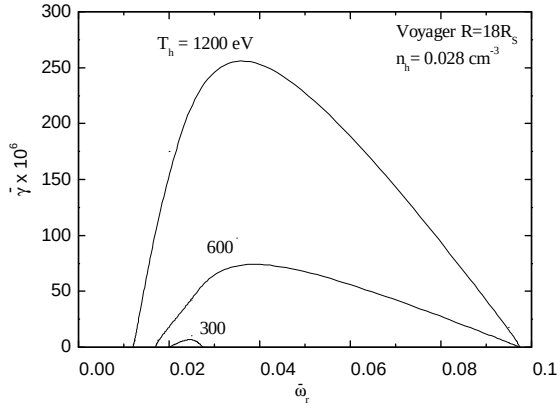

Fig. 6. Same as in Fig. 2 but for $R \sim 18\,R_S$.

effects of changing n_h and T_h, respectively at radial distance $12\,R_S$. Here the band width also increases with the increase in T_h but the effect is small in comparison with the case for radial distance $6\,R_S$. In Figs. 5 and 6 the effect of changing n_h or T_h, respectively, on the temporal growth rate is shown for radial distance $18\,R_S$. The change in bandwidth with changing n_h does not show any systematic trend. However, the effect of increasing T_h does result in somewhat larger bandwidth towards lower frequencies.

In Fig. 7 the effect of changing the parameter κ is shown at radial distance $5.5\,R_S$. The growth rate decreases with increasing κ, as is expected, since for higher κ, there are a lower number of resonant electrons in the high energy tail of the distribution function. Also, the bandwidth of the whistler mode emissions increases towards lower frequencies as κ is decreased.

In Fig. 8 the effect of hot electron anisotropy A_h on the growth rate is shown (R=$5.5\,R_S$). As the anisotropy is increased the growth rate increases considerably and the bandwidth also increases towards higher frequencies.

Finally, in Fig. 9, the results of the growth rate calculation for radial distance $3.9\,R_S$ are shown. It is found that for $n_h < 0.5\,\mathrm{cm}^{-3}$, no whistler mode emissions are possible. Also, the bandwidth of whistler mode emissions increases towards lower frequencies as n_h is increased to $1\,\mathrm{cm}^{-3}$. Furthermore, for radial distance $2.2\,R_S$ calculations produce no whistler mode emissions.

4.2 Comparisons with Cassini and Voyager observations

Next we compare our calculated values of the whistler mode emission frequency $\bar{\omega_r}(=\omega_r/\Omega_e)$ with the observed values from Cassini (Gurnett et al., 2005). From Fig. 3 of their work we note that whistler mode emissions were observed inside $6\,R_S$ at $\bar{\omega_r} \sim 0.15$ at ($R \sim 5.5\,R_S$), 0.05 ($R \sim 3.9\,R_S$) and 0.01 ($R \sim 2.2\,R_S$). From Fig. 8 ($R \sim 5.5\,R_S$) we observe that whistler mode emissions at this location can be reconciled with a temperature anisotropy $A_h > 0.15$. From Fig. 9 ($R \sim 3.9\,R_S$) it is noted that the whistler mode emission observed by Cassini require a hot electron number density of $n_h > 0.5\,\mathrm{cm}^3$. However, the whistler mode emission observed by Cassini at radial distance $2.2\,R_S$ cannot be pro-

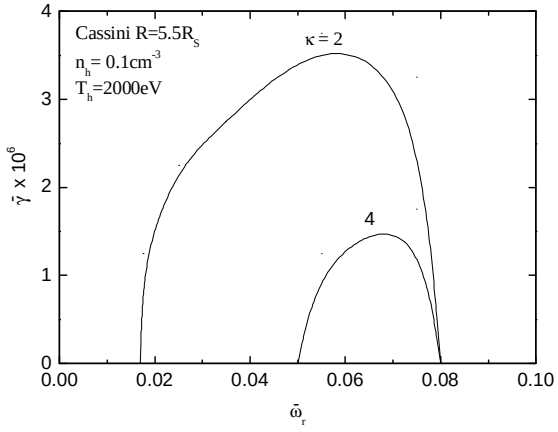

Fig. 7. Same as in Fig. 1 using plasma parameters for $R \sim 5.5\,R_S$ given in Table 2 (Cassini data). Parameter κ is marked.

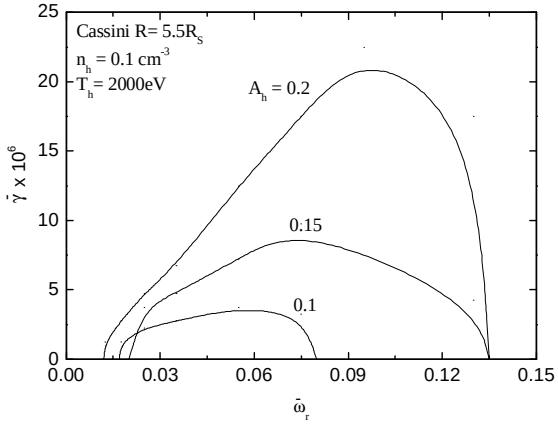

Fig. 8. Same as in Fig. 7. Hot (suprathermal) electron temperature anisotropy A_h is marked.

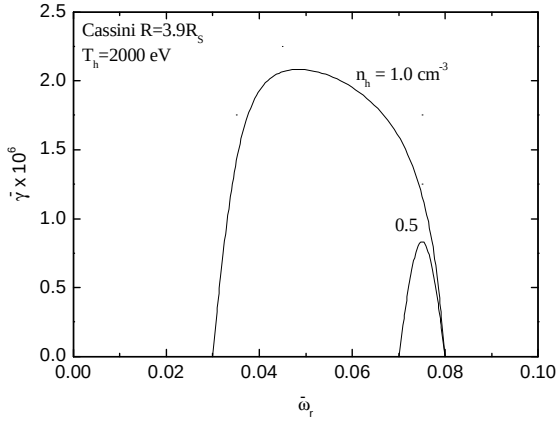

Fig. 9. Same as in Fig. 7 but for $R \sim 3.9\,R_S$. Hot (suprathermal) electron density n_h is marked.

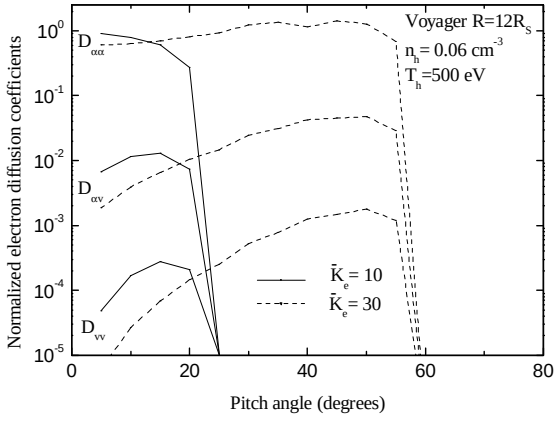

Fig. 10. Normalized electron diffusion coefficients versus pitch angle using temporal growth rate profile for $R \sim 12\,R_S$ (Fig. 3, n_h=0.06 cm^{-3}).

duced by our calculations as these will require energetic electron component with a much larger resonant energy of $E_r = \mathrm{B}_0^2/8\pi\,\mathrm{n_e}$.

Comparing our calculations with whistler mode wave observations by Voyager 1 (Fig. 3 of Gurnett et al., 1981), the broad-band emissions near ring plane crossing at 04:14 SCET (Space event time) on day 318 can be reproduced well by our calculations, as shown in Figs. 1 and 2. In this case the resonant energy of suprathermal electrons is small $\sim$1 keV. However, the observed whistler mode emissions on day 317 cannot be reproduced in our calculations, since a large resonant energy is required in this case. For the same reasons we also cannot reproduce whistler mode emissions observed by Voyager 2.

The present calculations do not reproduce the whistler mode emissions observed by Cassini at radial distance 2.2 R_S and by Voyager 1 on day 317 and by Voyager 2. The reason for this may be two-fold. Firstly, the present calculations use a linear theory which may not be applicable. Second, a more likely reason may be the fact that the whistler mode emissions observed in these cases may have been produced at more favourable (lower E_r) locations and then propagated to the location where these have been observed.

5 Electron diffusion coefficients

A whistler mode emission can cause pitch angle and energy diffusion of magnetospheric electrons and scatter them into the planet's atmosphere, thereby producing auroral emissions. On Saturn, aurora has been observed at high magnetic latitudes (Sandel and Broadfoot, 1981), suggesting a source of particles in the outer magnetosphere. It has been noted by Barbosa (1990) that keV electrons are most likely the primary precipitation energy source for the aurora. We have therefore calculated the pitch angle and energy diffusion coefficients, using two representative temporal growth rate pro-

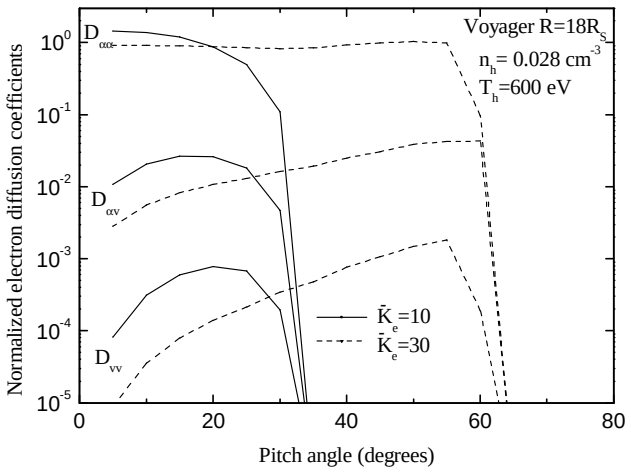

Fig. 11. Same as in Fig. 10 but for $R \sim 18\,R_S$ (using temporal growth rate profile from Fig. 5, n_h=0.028 cm^{-3}).

files; (1) at radial distance 12 R_S (Fig. 3, n_h=0.06 cm^{-3}) and (2) at radial distance 18 R_S (Fig. 5, n_h=0.028 cm^{-3}).

In Figs. 10 and 11 we show the normalized pitch angle and energy diffusion coefficients for electron interactions with whistler mode waves. Calculations have been performed using the diffusion coefficient expressions given by Lyons (1974). For the sake of completeness we give the details of these expressions and calculations in the Appendix. The electron energies for $\bar{K}_e$=10 and 30 at radial distance 12 R_s(Fig. 10) are ∼9 keV and 27 keV, respectively. The average pitch-angle diffusion coefficients $\langle \mathcal{D}_{\alpha\alpha} \rangle$ at these energies are 0.9 and 1.1, respectively. At radial distance 18 R_s (Fig. 11) the electron energies are 7 keV and 21 keV and average $\langle \mathcal{D}_{\alpha\alpha} \rangle$ values are 1.1 and 0.9, respectively. From Figs. 10 and 11 it is noted that the energy diffusion coefficients $\mathcal{D}_{\alpha v}$ and $\mathcal{D}_{vv}$ are several orders of magnitude smaller than $\mathcal{D}_{\alpha\alpha} \times v^2/\langle \mathcal{D}_{\alpha\alpha} \rangle$ (cf. Eq. A1) gives the time scale for pitch-angle diffusion $\tau_{\alpha\alpha}$. For a wave magnetic field intensity $B_{\rm wave}$=10^{-3} nT values of $\tau_{\alpha\alpha}$ at R=12 R_s are 7.7×10^4 s and 6.3×10^4 s for electron energies 9 keV and 27 keV, respectively. At R=18 R_s these are 2.3×10^4 s and 2.8×10^4 s for electron energies 7 keV and 21 keV respectively. It is useful to compare $\tau_{\alpha\alpha}$ with the "strong" pitch-angle diffusion time constant τ_{SD}. In the strong diffusion regime, particles diffuse across the loss cone in less than a quarter-bounce period, with the result that the precipitation mechanism saturates and the particle flux is driven isotropic. The particle precipitation rate is then independent of the amplitude of the scattering waves, and depends only on the particle bounce time and the geometric size of the loss cone. τ_{SD} is given approximately by Thorne (1983)

$$\tau_{SD} = 3.6\, R_s L^4/v, \tag{9}$$

where L is the magnetic shell parameter. Values of τ_{SD} at L=12 are 8×10^4 s and 4.6×10^4 s for 9 keV and 27 keV, respectively. At L=18 these are 4.6×10^5 s and 2.7×10^5 s for 7 keV and 21 keV, respectively. Thus, to set tens of keV electrons on strong diffusion ($\tau_{\alpha\alpha} \approx \tau_{SD}$) the wave amplitude must be about 10^{-3} nT at R=12 R_s and about 2−3×10^{-4} nT at R=18 R_s.

Electric fields of the whistler mode waves measured by Voyager 1 (Gurnett et al., 1981) are of the order of 10^{-6} V/m. Calculated group velocities v_g=$(d\omega/dk)$ are ∼ 6×10^6 m/s at R=12 R_s and ∼4×10^6 m/s at R=12 R_s. These give the magnetic field intensities of the waves (B=E/v_g) as 1.6×10^{-4} nT and 2.5×10^{-4} nT at R=12 R_s and 18 R_s, respectively. It may therefore be concluded that the whistler mode wave amplitudes may be sufficient to drive resonant electrons (tens of keV) onto strong diffusion at R=18 R_s, leading to intense precipitation into the atmosphere. At R=12 R_s, the wave intensity is insufficient to set keV electrons on strong diffusion.

6 Discussion and conclusion

We have applied the dispersion relation for parallel propagating whistler mode waves to the magnetosphere of Saturn and have made comparisons with the observations from Voyager and Cassini. Whistler mode emission observed by Voyager 1 near the ring plane crossing can be accounted for by our calculations. It is found that for a higher hot electron number density and/or temperature, the whistler mode emission covers a broadband of frequencies, especially toward lower frequencies. When the hot electrons are of low density or lower temperature, the emission is confined to a narrower range of frequencies. These findings are in very good agreement with the observations (Sittler et al., 1983). However, for hot electron density less than 0.5 cm^{-3} and a hot electron temperature <200 eV at radial distance 6 R_S no whistler mode emissions are obtained. The whistler mode emissions observed by Cassini at radial distance 5.5 R_S and 3.9 R_S can be reproduced well. However, at radial distance 3.9 R_S, a somewhat larger hot electron density than observed is needed.

Barbosa and Kurth (1993) have also analysed the whistler mode emissions in the inner magnetosphere of Saturn, using a power-law electron distribution function having pitch-angle anisotropy. These authors conclude that the suprathermal electron flux with pitch angle anisotropy M=1/2 can produce whistler-mode waves below $\omega/\Omega_e \approx 1/3$ in the vicinity of the magnetic equator. This is in agreement with the results of our calculations. Leubner (1982) has studied the whistler mode emissions on Jupiter, using an approximate expression for wave growth for a plasma consisting of thermal and suprathermal components described by Maxwellian and by a kappa distribution function, respectively. It is found in his work that the structure of the whistler mode hiss and chorus can be explained by the superposition of thermal and suprathermal components. In the present work we obtain a broad distribution of wave growth which does not resolve

into hiss and chorus (cf. Figs. 1–9). The difference between the wave growth results of the present calculations and that by Leubner (1982) may lie in the use of different expressions for dispersion relations used in the two works and the different manners in which the cold and hot electron components have been treated in the two calculations.

We have also calculated the pitch angle and energy diffusion coefficients at two radial distances R=12 R_s and 18 R_s, using the diffusion coefficient expression given by Lyons (1974). The details of the expressions and calculations are given in the Appendix. The time constants ($\tau_{\alpha\alpha}$) for pitch-angle diffusion for the assumed wave magnetic field intensity B_{wave}=10^{-3} nT are 7×10^4 s at R=12 R_s and 2.5×10^4 s at R=18 R_s. Comparing these time constants with the strong diffusion time constant τ_{SD} we conclude that the observed amplitudes of whistler mode emissions may be sufficient to drive tens of keV resonant electrons onto strong diffusion at R=18 R_s, leading to intense precipitation into the atmosphere. At R=12 R_s the observed wave intensity is, however, insufficient.

Appendix A

Expressions for electron diffusion coefficients

Following Lyons (1974), the normalized diffusion matrix $\mathcal{D}$ is defined as

$$\mathcal{D} = \mathbf{D}\left[\Omega_e \frac{B^2_{\rm wave}}{B^2_0} v^2\right]^{-1}, \tag{A1}$$

where v is electron speed, $\mathbf{D}$ is the diffusion matrix and $B_{\rm wave}$ is the wave magnetic field. Each element of the matrix is written as a sum over all resonances n and an integral over x

$$\mathcal{D} = \sum_{n=-\infty}^{\infty} \int_0^{x_{\max}} x dx \mathcal{D}^{nx}, \tag{A2}$$

where x=tan θ and θ is the wave normal angle (the angle between B_0 and k). $\mathcal{D}^{nx}$ is given by

$$\mathcal{D}^{nx}_{\alpha\alpha} = \frac{\pi cos^5\theta \Omega_e(-\sin^2\alpha - n\Omega_e/\omega_k)^2 \cdot |\Phi_{n,k}|^2}{2C_1\psi^{3/2}|1+n\Omega_e/\omega_k|^3 \cdot I(\omega_k)} \times f(\omega) g_\omega(x) \cdot \left(1 - \frac{1}{V_{||}} \frac{\partial\omega_k}{\partial k_{||}}\bigg|_x\right)\Bigg|_{\left(\frac{\omega_k}{\Omega_e}\right)=\left(\frac{\omega_k}{\Omega_e}\right)_{\rm res}}, \tag{A3}$$

where $f(\omega)$ is the wave spectral density and $g_\omega(x)$ gives the wave normal distribution. For $g_\omega(x)$ we use

$$g_\omega(x) \propto \exp(-x^2) \quad \text{for } x \le 1$$
$$0 \quad \text{for } x \ge 1. \tag{A4}$$

The wave spectral density is assumed to be proportional to the temporal growth rate. The constants of proportionality do not appear in the calculation of normalized diffusion coefficients. We have therefore used for $f(\omega)$ the temporal growth rates. In Eq. (A3), C_1=$\int f(\omega)d\omega$, α is the pitch-angle and

$$\left(1 - \frac{1}{V_{||}} \frac{\partial\omega_k}{\partial k_{||}}\bigg|_x\right) = 1-2\psi \left\{[1+n\Omega_e/\omega_k] \times \left[2\psi + 2\frac{\omega^2}{\Omega_p\Omega_e} - \frac{\omega^2}{\Omega_p^2}(1-M)^2 \times \left\{(1+x^2)\left(\psi - 1 + \frac{\omega^2}{\Omega_p\Omega_e}\right) + \frac{x^2}{2}\right\}^{-1}\right]\right\}^{-1}, \tag{A5}$$

$$|\Phi_{n,k}|^2 = \left[\left(\frac{D}{\mu^2-S}\right)^2 \left(\frac{\mu^2\sin^2\theta - P}{\mu^2}\right)^2 + \left(\frac{P\cos\theta}{\mu^2}\right)^2\right]^{-1} \times \left[\frac{\mu^2\sin^2\theta - P}{2\mu^2}\left(1 + \frac{D}{\mu^2-S}\right) J_{n+1} + \frac{\mu^2\sin^2\theta - P}{2\mu^2} \times \left(1 - \frac{D}{\mu^2-S}\right) J_{n-1} + \cot\alpha \sin\theta\cos\theta J_n\right]^2, \tag{A6}$$

$$I(\omega) = \int_0^\infty g_\omega(x) x \{(1+x^2)\psi\}^{-3/2} \times \left\{1 + \frac{1}{\psi}\left[\frac{\omega^2}{\Omega_p\Omega_e} - \left\{\frac{1}{2}\frac{\omega^2}{\Omega_p^2}(1-M)^2\right\} \times ;\left\{(1+x^2)\left(\psi - 1 + \frac{\omega^2}{\Omega_p\Omega_e}\right) + \frac{x^2}{2}\right\}^{-1}\right]\right\} dx \tag{A7}$$

Argument of Bessel function J_n=$J_n\left(x\tan\alpha\left(-\frac{\omega_k}{\Omega_e} - n\right)\right)$.

$$\mu^2 = \frac{\omega^2_{pe}}{\Omega^2_e}\frac{1+M}{M}\psi^{-1}, \tag{A8}$$

$$M = m_e/m_p, \tag{A9}$$

$$\psi = 1 - \frac{\omega_k^2}{\Omega_p\Omega_e} - \frac{\sin^2\theta}{2} + \left[\frac{\sin^4\theta}{4} + \left(\frac{\omega_k}{\Omega_p}\right)^2 (1-M)^2\cos^2\theta\right]^{1/2}, \tag{A10}$$

$$P = -\frac{\omega^2_{pe}}{\Omega^2_e}\frac{\Omega^2_e}{\omega^2_k}(1+M), \tag{A11}$$

$$S = \frac{1}{2}(R+L), \tag{A12}$$

$$D = \frac{1}{2}(R-L), \tag{A13}$$

$$\left.\begin{matrix} R \\ L \end{matrix}\right\} = \pm \frac{\omega_{pe}^2}{\Omega_e^2} \frac{\Omega_e}{\omega_k} \left[\frac{1+M}{1-M \mp (\omega_k/\Omega_e - \Omega_p/\omega_k)}\right], \quad \text{(A14)}$$

$$\mathcal{D}_{\alpha v}^{nx} = \mathcal{D}_{v\alpha}^{nx}$$

$$= \mathcal{D}_{\alpha\alpha}^{nx} \left[\frac{\sin\alpha\,\cos\alpha}{-\sin^2\alpha - n\,\Omega_e/\omega_k}\right]_{|\,(\omega_k/\Omega_e) = (\omega_k/\Omega_e)_{\rm res}}, \quad \text{(A15)}$$

$$\mathcal{D}_{vv}^{nx} = \mathcal{D}_{\alpha\alpha}^{nx} \left[\frac{\sin\alpha\,\cos\alpha}{-\sin^2\alpha - n\,\Omega_e/\omega_k}\right]^2_{|(\omega_k/\Omega_e) = (\omega_k/\Omega_e)_{\rm res}}. \quad \text{(A16)}$$

In Eqs. (A3), (A15) and (A16) the resonance frequency $(\omega_k/\Omega_e)_{res}$ is obtained as a function of x from

$$\bar{K}^e_{||,\rm res} = \frac{m_e}{m_p} \frac{(1+n\Omega_e/\omega_k)^2\psi}{\cos^2\theta(1+M)}, \quad \text{(A17)}$$

where $\bar{K}^e_{||,\rm res}$ is the normalized resonant parallel energy (parallel to the ambient magnetic field) given by

$$\bar{K}^e_{||} = \frac{K^e_{||}}{B_0^2/8\pi\, n_e} \quad \text{(A18)}$$

where $K^e_{||}$ is the parallel energy of the electron.

Calculations are performed for a given resonance energy $\bar{K}^e_{res}$, pitch angle α and for a given wave spectral density (temporal growth rate) $f(\omega)$. Using Eq. (A17), the resonance frequencies are obtained as a function of x. The calculation of normalized diffusion coefficients $\mathcal{D}$ is then performed using the algebraic expressions as given above. The summation over n in Eq. (A2) is performed for $|n| \leq 5$. Finally, the pitch-angle diffusion coefficient $\mathcal{D}_{\alpha\alpha}$ is averaged over pitch angle α

$$\langle \mathcal{D}_{\alpha\alpha} \rangle = \frac{1}{\alpha_{\rm max}} \int_0^{\alpha_{\rm max}} \mathcal{D}_{\alpha\alpha} d\alpha. \quad \text{(A19)}$$

Acknowledgements. This work was supported by a research associateship award to A. K. Tripathi by the Council of Scientific and Industrial Research, Government of India. Calculations reported in the present work were carried out at the Computer Centre, Banaras Hindu University.

Topical Editor I. A. Daglis thanks G. Hospodarsky and another referee for their help in evaluating this paper.

References

Barbosa, D. D.: Auroral precipitation flux of ions and electrons in Saturn's outer magnetosphere, Planet. Space Sci., 38, 1295–1304, 1990.

Barbosa, D. D. and Kurth, W. S.: On the generation of plasma waves in Saturn's inner magnetosphere, J. Geophys. Res., 98, 9351–9356, 1993.

Fried, B. D. and Conte, S. D.: The plasma dispersion function, Academic, 1961.

Gurnett, D. A., Kurth, W. S., Hospodarsky, G. B., et al.: Radio and plasma wave observations at Saturn from Cassini's approach and first orbit, Science, 307, 1255–1259, 2005.

Gurnett, D. A., Kurth, W. S., and Scarf, F. L.: Plasma waves near Saturn: Initial results from Voyager 1, Science, 212, 235–239, 1981.

Leubner, M. P.: On Jupiter's whistler emission, J. Geophys. Res., 87, 6335–6338, 1982.

Lyons, L. R.: Pitch angle and energy diffusion coefficients from resonant interactions with ion-cyclotron and whistler waves, J. Plasma Phys., 12, 417–432, 1974.

Mace, R. L.: Whistler instability enhanced by suprathermal electrons within the Earth's foreshock, J. Geophys. Res., 103, 14 643–14 654, 1998.

Sandel, B. R. and Broadfoot, A. L.: Morphology of Saturn's aurora, Nature, 292, 679–682, 1981.

Scarf, F. L., Gurnett, D. A., Kurth, W. S., et al.: Voyager 2 Plasma wave observations at Saturn, Science, 215, 587–594, 1982.

Sittler Jr., E. C., Ogilvie, K. W., and Scudder, J. D.: Survey of low-energy plasma electrons in Saturn's magnetosphere: Voyagers 1 and 2, J. Geophys. Res., 88, 8847–8870, 1983.

Summers, D. and Thorne, R. M.: The modified plasma dispersion function, Phys. Fluids B, 3, 1835–1847, 1991.

Summers, D. and Thorne, R. M.: plasma microinstabilities driven by loss-cone distributions, J. Plasma Phys., 53, 293–315, 1995.

Throne, R. M.: Microscopic plasma processes in the Jovian magnetosphere, in Physics of the Jovian Magnetosphere, edited by: Dessler, A. J., Cambridge University Press, NewYork, 454–488, 1983.

Young, D. T., Young, D. T., Berthelier, J. J., Blanc, M., et al.: Composition and dynamics of plasma in Saturn's magnetosphere, Science, 307, 1262–1265, 2005.